Journal of Magnetic Resonance 196 (2009) 1–6

Contents lists available at ScienceDirect

Journal of Magnetic Resonance

journal homepage: www.elsevier.com/locate/jmr

Globally optimal superconducting magnets Part I: Minimum stored energy (MSE) current density map

Quang M. Tieng, Viktor Vegh *, Ian M. Brereton

Centre for Magnetic Resonance, The University of Queensland, Level 2 Gehrmann Laboratories Research Road, Brisbane, St. Lucia, Qld 4072, Australia

ARTICLE INFO

Article history:
Received 30 June 2008
Revised 2 September 2008
Available online 26 September 2008

Keywords:
Current density map
Global optimization
Superconducting magnet
Quadratic programming

ABSTRACT

An optimal current density map is crucial in magnet design to provide the initial values within search spaces in an optimization process for determining the final coil arrangement of the magnet. A strategy for obtaining globally optimal current density maps for the purpose of designing magnets with coaxial cylindrical coils in which the stored energy is minimized within a constrained domain is outlined. The current density maps obtained utilising the proposed method suggests that peak current densities occur around the perimeter of the magnet domain, where the adjacent peaks have alternating current directions for the most compact designs. As the dimensions of the domain are increased, the current density maps yield traditional magnet designs of positive current alone. These unique current density maps are obtained by minimizing the stored magnetic energy cost function and therefore suggest magnet coil designs of minimal system energy. Current density maps are provided for a number of different domain arrangements to illustrate the flexibility of the method and the quality of the achievable designs.

1. Introduction

The utility of NMR and MRI imaging technology depends upon the magnetic field linearity and apparatus sensitivity, which in turn determines the quality and rate of acquisition of useful data. This consequently defines the spatial resolution of the image and associated rate of temporal data acquisition. In the case of magnetic resonance excitation of objects to generate images, the pursuit of higher sensitivity has resulted in a push to higher static magnetic field strengths, and at the same time, the requirement of higher RF resonator frequencies. The focus of this work is on the development of improved NMR and MRI static superconducting magnets to be used within the clinical and research environments [1].

The design of superconducting magnets has been widely investigated in the past using different optimization strategies to obtain coil layouts that produce predefined magnetic field linearity properties within a specified region and associated stray field characteristics. Optimization methods previously employed may be considered as one of two general approaches: either where a broad parameter space is searched for an optimal coil layout [2–5], or where initial constraints are placed on the optimization strategy to enable the calculation of a solution either more efficiently, or in a more convergent and stable manner [6–8]. The former tends to be associated with optimization strategies that require large computational resources, and the latter tends to achieve magnet coil layouts faster given favourable initial coil layout approximation or seed data. Recently, it has been shown that the different optimization strategies tend to provide very similar results, irrespective of the search space [9].

The literature suggests that it is possible to obtain better superconducting magnet coil layouts using more appropriate strategies in different domains [10]. The approach described here promotes the concept of a unique coil layout being derived from a fundamental current density map. The process of achieving a final magnet design requires two individual key steps: definition of the initial coil layout and then final optimization of the magnet coil arrangement. In Part I of this work, we outline the process of obtaining the globally minimum stored energy current density map from which an initial coil layout is obtained. In a following publication, Part II [11], the second step in the process is described whereby the magnet arrangement is generated from the fundamental current density map. It should be noted that in this work superconducting coils are treated as cylindrical structures with coaxial symmetry allowing current density maps to be described over a two-dimensional domain.

2. Background theory

The magnetic field produced by an arbitrarily shaped electric current carrying conductor cell can be expressed as the sum of an infinite series of spherical harmonics. The amplitude and sign of each spherical harmonic expansion term depends on the cell geometry, current strength, winding direction and relative posi-

* Corresponding author. Fax: +61 7 3365 3833.
E-mail address: v.vegh@uq.edu.au (V. Vegh).

1090-7807/$ - see front matter
doi:10.1016/j.jmr.2008.09.018

tions of cells in a particular domain configuration. Hence, a collective set of cells expressed in terms of spherical harmonics can be arranged in space to satisfy design specific constraints, through appropriate choice of size, current magnitude/direction and spacing. Therefore, spherical harmonic expansions are used to define individual current carrying cells to reduce the computational cost and overall optimization complexity.

Fig. 1 depicts the defined geometry and reference frame for a cell in space, where the inherent symmetry is assumed to characterize the cylindrical nature of the system, and allows for simplification to only two dimensions. The z-axis is assumed to be the longitudinal axis aligned with B_0, and also the direction in which subjects to be examined are inserted, for example, in Magnetic Resonance Imaging (MRI) or Nuclear Magnetic Resonance (NMR) spectroscopy magnets.

The axial component of the magnetic field at a point $(r < r_0,\theta)$ in an axisymmetric configuration comprising filament current carrying circular cells coaxial with the z-axis is in general given by [12]:

$$B_z(r < r_0,\theta) = I\sum_{n=1}^{\infty} a_n P_{n-1}(\cos\theta) r^{n-1}, \tag{1}$$

where

$$a_n = -\frac{\mu_0}{2}\sin\ \theta_0 \frac{P_n^1(\cos\ \theta_0)}{r_0^n}$$

In (1) μ_0 is the permeability of free space, I is the cell current density, $(r_0,\ \theta_0)$ defines the cell geometry with respect to an arbitrary origin, $(r,\ \theta)$ is the field point with respect to the origin and $P_n^m(\cos\ \theta)$ is the associated Legendre polynomial evaluated at the appropriate location in space.The corresponding field expansion for points lying in the external region defined for $r > r_0$ is given by [12]:

$$B_z(r > r_0,\theta) = I\sum_{n=1}^{\infty} b_n \frac{P_{n+1}(\cos\ \theta)}{r^{n+2}}, \tag{2}$$

where

$$b_n = -\frac{\mu_0}{2}\sin\ \theta_0 P_n^1(\cos\ \theta)_0 r_0^{n+1}.$$

For more appropriate cell definitions, Eqs. (1) and (2) are extended to allow for the calculation of the magnetic field generated by a rectangular cross-section cell as:

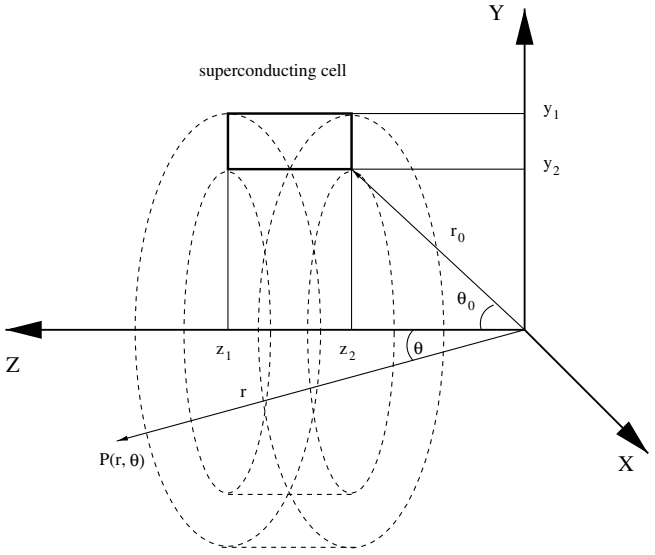

Fig. 1. Definition of the magnetic field at point $P(r,\theta)$ produced by a cylindrical superconducting cell with a cross-section in the yz-plane.

$$\begin{aligned} B_z\left(r < \sqrt{y_2^2+z_2^2},\theta\right) &= I\sum_{n=1}^{\infty}\alpha_n P_{n-1}(\cos\ \theta) r^{n-1}, \\ B_z\left(r > \sqrt{y_1^2+z_1^2},\theta\right) &= I\sum_{n=1}^{\infty}\beta_n \frac{P_{n+1}(\cos\ \theta)}{r^{n+2}}, \end{aligned} \tag{3}$$

where

$$\alpha_n = -\frac{\mu_0}{2}\int_{z_2}^{z_1}\int_{y_2}^{y_1}\frac{y}{\sqrt{y^2+z^2}}\frac{P_n^1\left(z/\sqrt{y^2+z^2}\right)}{\left(y^2+z^2\right)^{\frac{n}{2}}}dydz,$$

$$\beta_n = -\frac{\mu_0}{2}\int_{z_2}^{z_1}\int_{y_2}^{y_1}\frac{y}{\sqrt{y^2+z^2}}P_n^1\left(\frac{z}{\sqrt{y^2+z^2}}\right)\left(y^2+z^2\right)^{\frac{n+1}{2}}\mathrm{d}y\mathrm{d}z.$$

In (3) coordinates (y_1,z_1) and (y_2,z_2) define the rectangular conductor cross-section in the yz-plane as shown in Fig. 1. The harmonic coefficients α_n and β_n can be computed analytically or numerically. The analytic expressions for the coefficients can be obtained by solving the integral for α_n and β_n, but rather Gaussian quadrature [13] was used in the general implementation to obtain the individual values of α_n and β_n. The procedure of using Gaussian quadrature was found to be both accurate and efficient, when compared to the analytic expressions. Nevertheless for reference, the first two harmonic coefficients for the inner region given in analytical form are:

$$\alpha_1 = -\frac{\mu_0}{2}\left[z_1\ln\left(\frac{y_2+\sqrt{y_2^2+z_1^2}}{y_1+\sqrt{y_1^2+z_1^2}}\right)+z_2\ln\left(\frac{y_1+\sqrt{y_1^2+z_2^2}}{y_2+\sqrt{y_1^2+z_2^2}}\right)\right],$$

$$\alpha_2 = -\frac{\mu_0}{2}\left[y_1\left(\frac{1}{\sqrt{y_1^2+z_2^2}}-\frac{1}{\sqrt{y_1^2+z_1^2}}\right)-y_2\left(\frac{1}{\sqrt{y_2^2+z_2^2}}-\frac{1}{\sqrt{y_2^2+z_1^2}}\right)\right] - \frac{\mu_0}{2}\ln\left(\frac{(y_1+\sqrt{y_1^2+z_1^2})(y_2+\sqrt{y_2^2+z_2^2})}{(y_1+\sqrt{y_1^2+z_2^2})(y_2+\sqrt{y_2^2+z_1^2})}\right),$$

and for the outer region:

$$\beta_1 = -\frac{\mu_0}{2}\left[\frac{1}{3}\left(y_1^3-y_2^3\right)(z_2-z_1)\right],$$
$$\beta_2 = -\frac{\mu_0}{2}\left[\frac{1}{2}\left(y_1^3-y_2^3\right)\left(z_2^2-z_1^2\right)\right].$$

3. MSE current density map

The static magnetic field is divided into the inner and outer field regions, to allow for the calculation of the field using the spherical harmonic method. If the conductors lie within a spherical shell centred at the origin, then the inner field is defined to be the space within the inner boundary and the outer field is therefore the space outside the outer boundary, as shown in Fig. 2. In the figure the cells used for calculating the current density map are illustrated in the top domain of the magnet, and the potential final coil arrangement based on the resultant current density map is depicted in the lower magnet domain for clarity.

The domain of interest is divided into K small cells or elements, as shown at the top corner of Fig. 2. The current densities I_k associated with individual cells are then determined by minimizing the cost function F, which is formulated as a stored energy sum:

$$\min_{I_k}\quad F = \frac{1}{2}\sum_{k=0}^{K-1} L_k I_k^2 A_k^2, \tag{4}$$

subject to:

$$\begin{aligned} &\sum_{k=0}^{K-1}\alpha_{k,1} I_k = B_0, \\ &\sum_{m=0}^{M-1}\sum_{k=0}^{K-1}\beta_{k,m} I_k = 0, \\ &\sum_{n=1}^{N-1}\sum_{k=0}^{K-1}\alpha_{k,n} I_k = 0, \\ &I_{\min} \leqslant I_k \leqslant I_{\max}, \end{aligned} \tag{5}$$

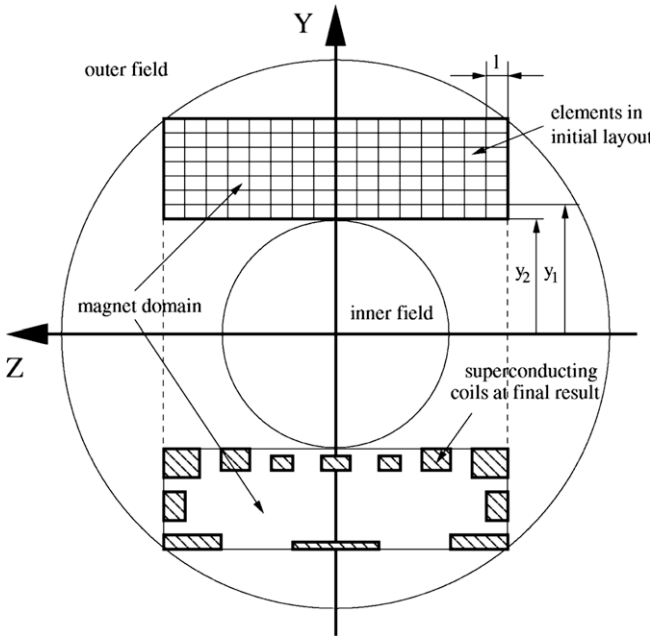

Fig. 2. Illustration of the domain of the magnet, and the inner and outer magnetic fields.

where

$$L_k = \frac{31.6\left((y_{k,1} - y_{k,2})y_{k,2}l_k/A_k\right)^2}{6y_{k,2} + 9l_k + 10(y_{k,1} - y_{k,2})}10^{-6}. \quad (6)$$

In (5) B_0 is the desired magnetic field strength at the iso-centre, $\alpha_{k,n}$ and $\beta_{k,m}$ are the spherical harmonic terms of element k, where M specifies the number of external harmonic coefficients and N the number of internal harmonic coefficients, under the condition that $K \geqslant M + N$. In (6) L_k is the self inductance of element k [14] with its dimensions shown in Fig. 2, and A_k is the cross-sectional area of the current carrying wire associated with the element. The values chosen for M and N define the size of the stray field and the Diameter Spherical Volume (DSV), respectively. Both M and N are increased to decrease the size of the stray field and to increase the size of the DSV. If a magnet design has N - 1 internal coefficients and M external coefficients vanished, then it is referred to as an N order M degree magnet design, to define a terminology of reference.

For magnet configurations in which coils are coaxial and symmetric about the illustrated xy-plane, the spherical harmonic expansion results in the elimination of all even order terms within the expansion. To further reduce computational complexity, the strategy employed here considers only one quarter of the magnet domain and thus the constraint (5) is simplified as follows:

$$\sum_{k=0}^{K-1} \alpha_{k,1} I_k = \frac{B_0}{2},$$

$$\sum_{n=1}^{N/2-1} \sum_{k=0}^{K-1} \alpha_{k,2n+1} I_k = 0, \quad (7)$$

$$\sum_{m=0}^{M/2-1} \sum_{k=0}^{K-1} \beta_{k,2m+1} I_k = 0,$$

$$I_{\min} \leqslant I_k \leqslant I_{\max},$$

where, K is the number of elements in one quarter of the magnet domain.

The cost function provided in Eq. (4) is formulated as the stored energy of K elements in the magnet domain. The optimization methodology ensures that the stored energy is minimized, and consequently, magnet training and quenching strains as a result of stored magnetic energy will be kept to a minimum in the final design. However, we would like to point out that the minimum stored energy is not our primary aim, but rather our goal is to minimize both the volume of the superconductor and the coil current density, which are equivalent to minimizing the stored energy of individual coils. If an accurate calculation of the stored energy was required, then the mutual inductance would have to be catered for and included as part of the cost function.

In Eqs. (4), (5), and (7) the parameters are constant except for I_k, since the cell geometries are fixed. The cost function is in quadratic form and the constraints are linear. Therefore, the problem can be solved using the general quadratic program (QP) [15]. The problem is stated as a strictly convex QP, since $L_k > 0$ and hence, the solution obtained using this procedure yields the global minimum, or the derived total stored energy has the smallest value. This is a very important observation with respect to the current density map, because this methodology allows designs to be obtained that are unique and cannot be improved using other methodologies for the same domain dimensions. The minimization of F generates unique, Minimum Stored Energy (MSE) current density maps, in which the coils are embedded as described in Part II of this work.

4. Results

The current density map has several local maxima and minima within the magnet domain, referred to as extremities. The number of extremities is proportional to the number of eliminated spherical harmonics, and notably these extremities lie around the perimeter of the magnet region. For longer magnet domains, the current density map may have a relatively large number of successive maxima and minima of a common polarity, such that positive maxima are adjacent to positive minima, and vice versa. As the length of the magnet region is reduced, the number of such extremities becomes smaller, with a further reduction in the size of the magnet domain resulting in the adjacent extremities having opposite polarities. This means that in compact designs, positive maxima are located adjacent to negative minima.

This section illustrates the location of the MSE current density map extremities and the distribution of these extremities as the size of the magnet domain is varied. Fig. 3 illustrates the concept described here for the example of a 3 m long magnet domain. The current density map illustrated in Fig. 3(a) is for an unshielded order 10 degree 0 design, and Fig. 3(b) is for the shielded order 10 degree 2 design. As depicted in Fig. 3, the current density extremities are located around the perimeter of the magnet domain to achieve a desired magnetic field. Both designs of Fig. 3(a) and (b) aim to achieve the same DSV size, but the design of Fig. 3(b) would have a significantly smaller stray field, since the external harmonic coefficients are considered. The current density map of Fig. 3(a) does not have any negative values, whereas in Fig. 3(b) negative minima are incorporated to reduce the stray field produced by the current carrying cells. This finding explains the general observation that in longer, or smaller DSV magnets, the winding directions are only in the positive sense, and that negative winding coils are introduced when active shielding is invoked.

As the length of the magnet domain is decreased, the minima start to take on negative values, which imply that negative windings are required to reduce the magnet length, as shown in Figs. 4 and 5. Fig. 4 depicts the current density map of order 14 and degree 0. If the domain is sufficiently long, then the extremities may

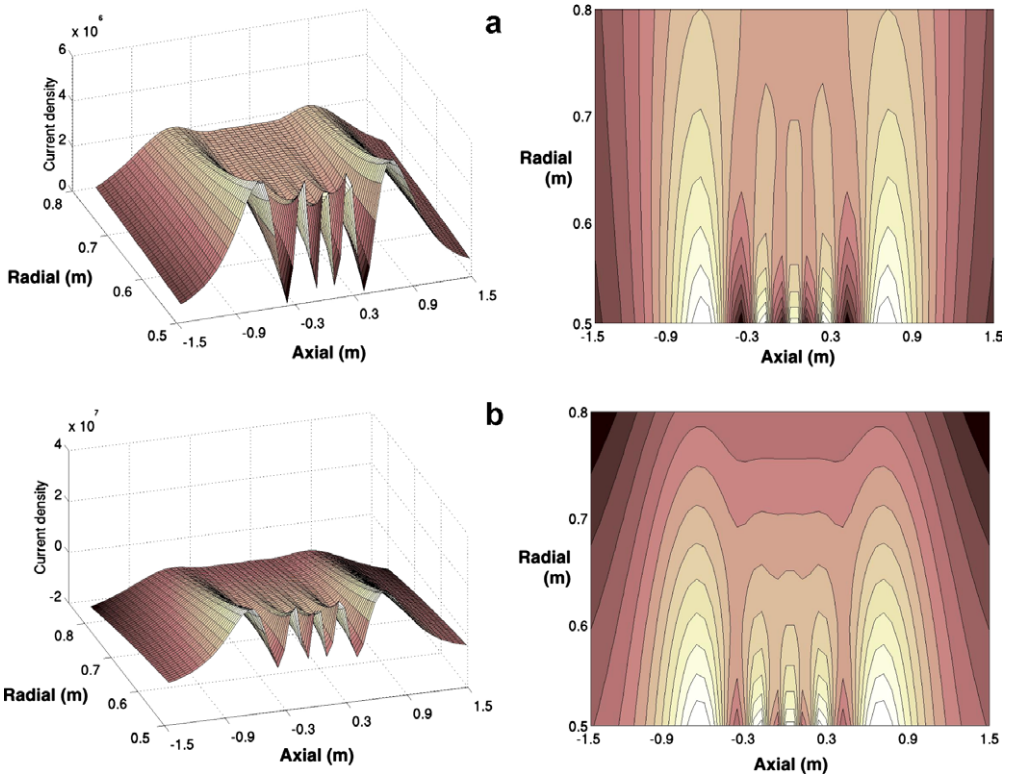

Fig. 3. MSE current density profiles with contours for (a) unshielded order 10 degree 0 and (b) shielded order 10 and degree 2 3 m long magnet domains.

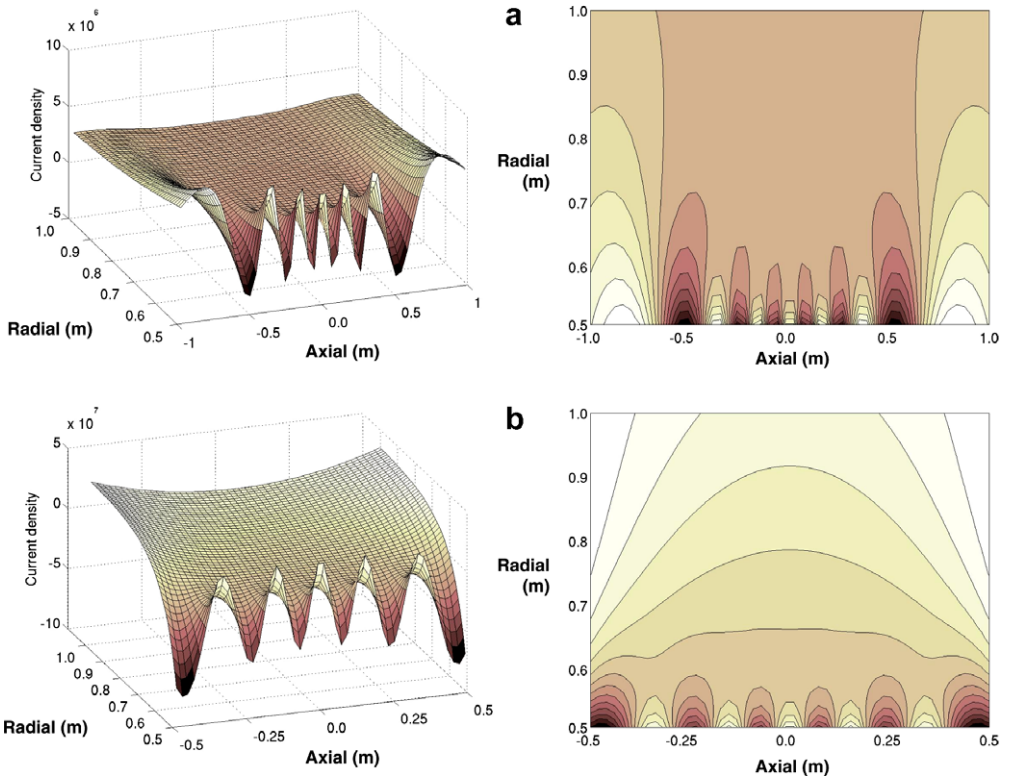

Fig. 4. MSE current density profiles with contours for the unshielded order 14 degree 0 (a) 2 m and (b) 1 m length magnet domains. The maximum peaks at the lower corners in (a) move to the outer boundary in (b) as the domain length is reduced.

only be positioned on the lower domain boundary, as can be seen in Fig. 4(a). Fig. 4(b) is an illustration of the effect upon the current density map, when the domain length is decreased to a length of 1 m. As can be seen by comparing Figs. 4(a) and (b), the extremities within the magnet domain still alternate in current direction, but wrap around the perimeter of the domain as it is shortened. As a

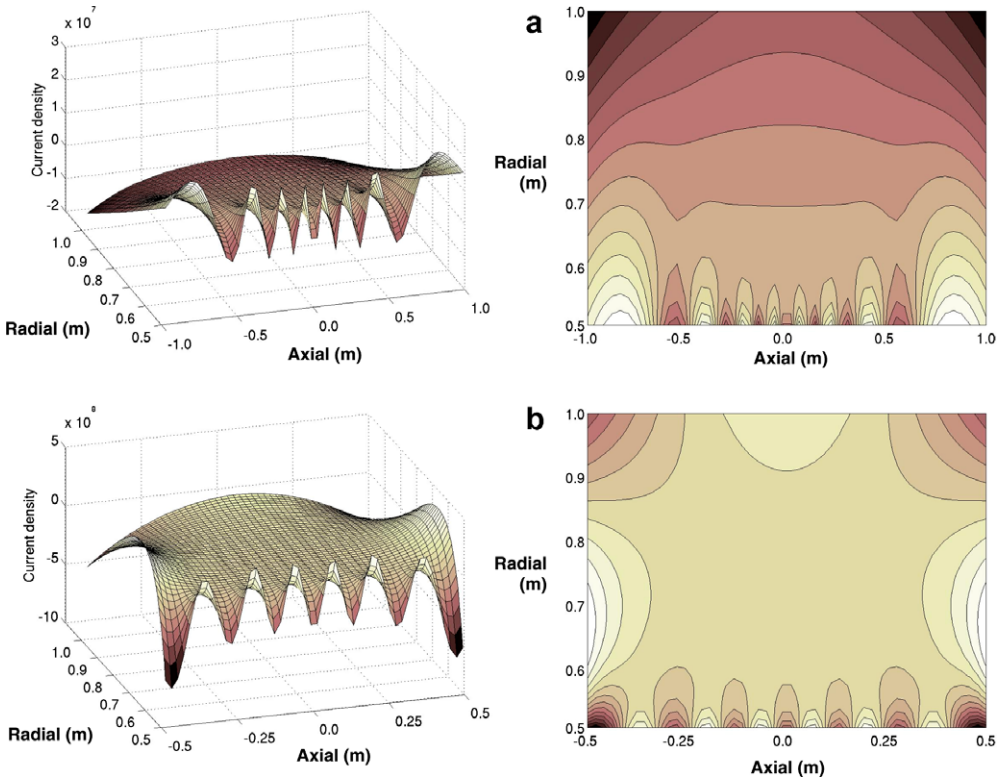

Fig. 5. MSE current density profiles with contours for the shielded order 16 degree 4 (a) 2 m and (b) 1 m length magnet domains.

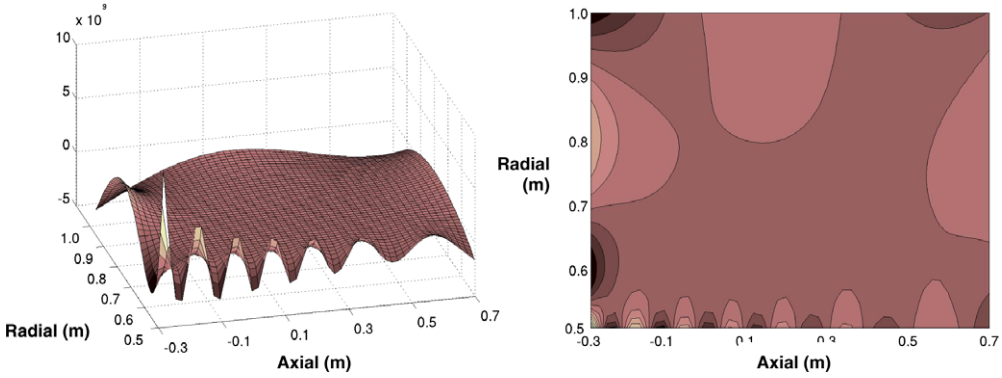

Fig. 6. MSE asymmetric current density profiles with contours for the shielded order 16 degree 4 1 m length magnet domain. The minima at the lower left hand corner in Fig. 5(b) have now moved to an upper layer as the DSV is shifted towards the left boundary of the magnet domain.

result, the individual coil locations are not restricted to the inner domain boundary.

In Fig. 5(a) the current density map for a shielded 2 m magnet is illustrated. Fig. 5(b) provides the current density map for the shortened designed. As can be seen in Fig. 5(a) and (b), the current density values theoretically indicate alternating extremities within the current densities within the magnet domain. Once again, the optimized current density map, as was in the case for the unshielded design, possesses extremities on the perimeter of the domain.

Fig. 6 illustrates the asymmetric current density map for a shielded 1 m magnet when the DSV is not located at the geometric iso-centre of the magnet. The MSE current density map again indicates alternating current density extremities located on the perimeter of the magnet domain. Comparison of Figs. 5(b) and 6 highlight that both designs have the same order, degree and magnet domain length, thus they also have the same number of extremities. However, the current density map becomes asymmetric and the extremities at the lower boundary in Fig. 5(b) are shifted in the direction in which the DSV origin has been moved.

5. Conclusions

The strategy of obtaining minimum stored energy MSE current density maps for various magnet domain configurations is described in detail. The current densities obtained illustrate that in an optimal design, the peak current densities are located around the perimeter of the magnet domain.

As the magnet domain is made shorter, the peak current densities tend to alternate in sign, while remaining on the perimeter of the magnet domain. As the magnet is made longer, the negative extremities disappear, yielding traditional positive turn superconducting magnet designs.

References

[1] G. Morrow, Progress in MRI magnets, IEEE Transactions on Applied Superconductivity 10 (2000) 744–751.
[2] N.R. Shaw, R.E. Ansorge, Genetic algorithms for MRI magnet design, IEEE Transactions on Applied Superconductivity 12 (2002) 733–736.
[3] H. Zhao, S. Crozier, D.M. Doddrell, A hybrid, inverse approach to the design of magnetic resonance imaging magnets, Medical Physics 27 (2000) 599–607.
[4] M.R. Thompson, R.W. Brown, V.C. Srivastava, An inverse approach to the design of MRI main magnets, IEEE Transactions on Magnetics 30 (1994) 108–112.
[5] A.K. Kalafala, A design approach for actively shielded magnetic resonance imaging magnets, IEEE Transactions on Magnetics 26 (1990) 1181–1188.
[6] Y.C.N. Cheng, T.P. Eagan, R.W. Brown, S.M. Shvartsman, M.R. Thompson, Design of actively shielded main magnets: an improved functional method, Magnetic Resonance Materials in Physics Biology and Medicine 16 (2003) 57–67.
[7] S. Crozier, D.M. Doddrell, Compact MRI magnet design by stochastic optimization, Journal of Magnetic Resonance 127 (1997) 233–237.
[8] H. Zhao, S. Crozier, D.M. Doddrell, Compact clinical MRI magnet design using multi-layer current density approach, Magnetic Resonance in Medicine 45 (2001) 331–340.
[9] Y.C.N. Cheng, R.W. Brown, M.R. Thompson, T.P. Eagan, S.M. Shvartsman, A comparison of two design methods for MRI magnets, IEEE Transactions on Applied Superconductivity 14 (2004) 2008–2014.
[10] B. Zhang, C. Gazdzinski, B.A. Chronik, H. Xu, S.M. Conolly, B.K. Rutt, Simple design guidelines for short MRI systems, Concepts in Magnetic Resonance Part B 25B (2005) 53–59.
[11] Q.M. Tieng, V. Vegh, I.M. Brereton, Globally optimal superconducting magnets Part II: minimum stored energy (MSE) coil arrangement, Journal of Magnetic Resonance (2008). vol. Under review.
[12] W.R. Smythe, Static and Dynamic Electricity, McGraw-Hill Book Company. Inc., New York, 1950.
[13] W.H. Press, S.A. Teukolsky, W.T. Vetterling, B.P. Flannery, Numerical Recipes in C: The Art of Scientific Computing, Second ed., Cambridge University Press, 2002.
[14] J.A. Edminister, Theory and Problems of Electromagnetics, McGraw-Hill Book Company, 1979.
[15] J. Nocedal, S.J. Wright, Numerical Optimization, Second ed., Springer, New York, 2006.